Wide Nanoscopic Pore of Maxi-Anion Channel Suits its Function as an ATP-Conductive Pathway

Ravshan Z. Sabirov and Yasunobu Okada
Department of Cell Physiology, National Institute for Physiological Sciences, Okazaki, Japan

ABSTRACT The newly proposed function of the maxi-anion channel as a conductive pathway for ATP release requires that its pore is sufficiently large to permit passage of a bulky ATP^{4-} anion. We found a linear relationship between relative permeability of organic anions of different size and their relative ionic mobility (measured as the ratio of ionic conductance) with a slope close to 1, suggesting that organic anions tested with radii up to 0.49 nm (lactobionate) move inside the channel by free diffusion. In the second approach, we, for the first time, succeeded in pore sizing by the nonelectrolyte exclusion method in single-channel patch-clamp experiments. The cutoff radii of PEG molecules that could access the channel from intracellular (1.16 nm) and extracellular (1.42 nm) sides indicated an asymmetry of the two entrances to the channel pore. Measurements by symmetrical two-sided application of PEG molecules yielded an average functional pore radius of ~1.3 nm. These three estimates are considerably larger than the radius of ATP^{4-} (0.57–0.65 nm) and $MgATP^{2-}$ (~0.60 nm). We therefore conclude that the nanoscopic maxi-anion channel pore provides sufficient room to accommodate ATP and is well suited to its function as a conductive pathway for ATP release in cell-to-cell communication.

INTRODUCTION

Adenosine triphosphate (ATP) is a universal source of energy for cellular functions which is constantly produced and consumed inside cells at a very high rate. A steep concentration gradient (several mmol in the cytosol versus nmol in the extracellular fluid) together with the transmembrane potential (negative in the cell) creates a highly favorable driving force for ATP release and its function as an ''extracellular second messenger''. Indeed, ATP signaling is a well-recognized event in cell-to-cell communication (Dubyak and El-Moatassim, 1993; Ralevic and Burnstock, 1998, 2003; Fields and Stevens, 2000; Hoebertz et al., 2003), and pathways for the regulated release of ATP are under intensive investigation (Novak, 2003; Schwiebert and Zsembery, 2003; Sabirov and Okada, 2004).

As most ATP molecules exist in anionic forms at physiological pH, it is plausible that an anion channel can electrogenically translocate ATP, thereby serving as a conductive pathway for ATP release. Many groups have proposed different chloride channels as candidates for an ATP release pathway. Patch-clamp studies revealed ATP-conducting currents in association with the expression of CFTR (Reisin et al., 1994; Schwiebert et al., 1995; Cantiello et al., 1997, 1998; Pasyk and Foskett, 1997; Lader et al., 2000; Cantiello, 2001) or that of MDR1 (Abraham et al., 1993; Bosch et al., 1996; Roman et al., 1997), and ATP currents independent of CFTR or MDR1 expression (Sugita et al., 1998; Bodas et al., 2000). Hisadome and collaborators (2002) suggested that ATP anions can permeate volume-sensitive outwardly rectifying (VSOR) anion channels in endothelial cells. However, we have demonstrated that neither the CFTR chloride channel nor the VSOR anion channel is involved in swelling-induced ATP release from human epithelial intestine 407 cells (Hazama et al., 1998, 1999) or mouse mammary C127 cells (Hazama et al., 2000).

Searching for a conductive pathway for ATP release, we have identified the swelling-activated Gd-sensitive Ohmic anion channel as a new candidate in mouse mammary C127 cells (Sabirov et al., 2001). The single-channel events we observed exhibited a large unitary conductance (300–400 pS) and voltage-dependent inactivation, both of which are characteristic to the maxi-anion channel. ATP produced a profound voltage-dependent blockage revealing an ATP-binding site in the middle of the pore accessible from both the extracellular and intracellular sides. The reversal potential measurements in the presence of only ATP^{4-} anions from the cytosolic side indicated a tangible ATP permeability with a P_{ATP}/P_{Cl} of 0.09. The pharmacological profile of single-channel activity was similar to that found for swelling-induced ATP release. Also, both swelling-induced ATP release and maxi-anion channel in these cells were found to be under negative control by intracellular arachidonic acid signaling (Dutta et al., 2002). In *macula densa* cells, a similar Gd-inhibitable maxi-anion channel was activated in response to an increase in the luminal NaCl concentration (Bell et al., 2003). The channel had a P_{ATP}/P_{Cl} of 0.14 and was suggested to serve as a conductive ATP release pathway for transducing signals from the *macula densa* to the adjacent mesangial cells during tubuloglomerular feedback in the kidney (Bell et al., 2003).

The hypothesis of ATP passing through the maxi-anion channel requires that the pore is sufficiently large to permit

Submitted March 18, 2004, and accepted for publication May 24, 2004.

Address reprint requests to Ravshan Z. Sabirov, Dept. of Cell Physiology, National Institute for Physiological Sciences, Myodaiji, Okazaki 444-8585, Japan. Tel.: 81-564-55-7733; Fax: 81-564-55-7735; E-mail: sabirov@nips.ac.jp.

0006-3495/04/09/1672/14 $2.00

doi: 10.1529/biophysj.104.043174

passage of a bulky ATP^{4-} and/or $MgATP^{2-}$ anion. Therefore, in the present study, we attempted to present a mechanistic view of the conducting pathway of the maxi-anion channel. We used two independent methods to estimate the size of the maxi-anion channel pore. First, we determined the permeability of the maxi-anion channel to a series of organic anions of different size. However, we found that even the largest organic anions tested permeated the channel with a rate close to their mobility in the solution, and that the size of the maxi-anion channel pore estimated by this method represents an underestimate. The nonelectrolyte partitioning method has been shown to be a reliable way to probe nanoscale pores and to yield estimates consistent with x-ray crystallography and electron microscopy data (reviewed by Krasilnikov, 2002; Bezrukov and Kasianowicz, 2002). However, the method requires very high concentrations of nonelectrolytes and so far has been restricted to experiments with planar lipid bilayers. Here, for the first time, we demonstrate applicability of this method to patch-clamp experiments and show that the pore of the maxi-anion channel is large enough to suit its function as an ATP-conductive pathway in cell-to-cell communication.

MATERIALS AND METHODS

Cells

A cell line of mouse mammary tissue origin, C127, was obtained from the American Type Culture Collection (Manassas, VA) and grown in Dulbecco's modified Eagle's medium (DMEM) containing 10% fetal calf serum (FCS). For patch-clamp experiments, the cells were grown on glass coverslips.

Chemicals

All organic anions were purchased as sodium salts from Sigma-Aldrich (St. Louis, MO). Polyethylene glycol (PEG) 3400 was from ICN Biomedicals (Aurora, OH). All other PEGs were from Wako Pure Chemical (Osaka, Japan).

Solutions

The control Ringer solution contained (mM): 135 NaCl, 5 KCl, 2 $CaCl_2$, 1 $MgCl_2$, 5 Na-HEPES, 6 HEPES, 5 glucose (pH 7.4, 290 mOsmol kg^{-1} H_2O). For bi-ionic selectivity measurements, pipette solution containing 150 mM NaCl and 5 mM HEPES (pH 7.4 adjusted with NaOH) and bath solution containing 150 mM sodium salt of the test anion supplemented with 5 mM HEPES (pH 7.4 adjusted with NaOH) were employed. For nonelectrolyte partitioning experiments, both pipette and bath solutions were control Ringer solution with or without 20% (wt/vol) test nonelectrolytes. Nonelectrolytes were added to premade control Ringer solution.

The osmolality of solutions was measured using a freezing-point depression osmometer (OM802, Vogel, Germany). The solution conductivity was measured at 25°C using a B-173 conductivity meter (Horiba, Kyoto, Japan). The viscosity of solutions containing nonelectrolytes was measured at 25°C with a capillary viscometer (Sibata, Tokyo, Japan).

Electrophysiology

Patch electrodes were fabricated from borosilicate glass capillaries using a laser micropipette puller (P-2000, Sutter Instrument, Novato, CA) and had a tip resistance of 2–5 MΩ when filled with pipette solution. Single-channel recordings were made using the excised, inside-out configuration of the patch-clamp technique. Membrane currents were measured with an EPC-9 patch-clamp system (HEKA-Electronics, Lambrecht/Pfalz, Germany) or an Axopatch 200A patch-clamp amplifier coupled to a DigiData 1200 interface (Axon Instruments, Foster, CA). The membrane potential was controlled by shifting the pipette potential (Vp). The membrane potential is reported as $-Vp$. Currents were filtered at 1 kHz and sampled at 5–10 kHz. Data acquisition and analysis were done using Pulse+PulseFit (HEKA-Electronics) or pCLAMP6 (Axon Instruments) and WinASCD software (provided by Dr. G. Droogmans, Katholieke Universiteit Leuven, Belgium). Whenever the bath Cl^- concentration was altered, a salt bridge containing 3 M KCl in 2% agarose was used to minimize variations of the bath electrode potential. In the experimental conditions used, the ionic composition of pipette and bath solutions did not generate any significant liquid junction potential error (app. 0.1 mV as calculated using pCLAMP8 algorithms), and therefore no correction was made. All experiments were performed at room temperature (23–25°C).

Data analysis

Single-channel amplitudes were measured by manually placing a cursor at the open and closed channel levels. The single-channel current-voltage (I–V) relationships in the presence of organic anions were fitted to the polynomial

$$I = A + B_1V + B_2V^2. \quad (1)$$

Reversal potentials (E_{rev}) were calculated from the quadratic equations

$$A + B_1V + B_2V^2 = 0, \quad (2)$$

$$E_{rev} = 2A/[-B_1 - (B_1^2 - 4B_2A)^{1/2}], \quad (3)$$

where V is the membrane potential, and A, B_1, and B_2 are the parameters of the polynomial fit.

Permeability ratios for different anions (X) were calculated from the Goldman-Hodgkin-Katz equation for bi-ionic conditions,

$$\Delta E_{rev} = -RT/F \ln(P_{Cl}a_{Cl}[Cl]_o)/(P_Xa_X[X]), \quad (4)$$

where ΔE_{rev} is the reversal potential with a test anion present in the bath at a concentration of $[X]$, $[Cl]_o$ represents the Cl^- concentration in the pipette solution, a_{Cl} and a_X are the corresponding activity coefficients, and P_{Cl} and P_X are the permeability coefficients of Cl^- and the test anion, respectively. In the present study, we calculated the permeability ratios on the assumption that all monovalent anions used have the same activity coefficient as Cl^-. This assumption seems to be reasonable, since activity coefficients for Cl^-, formate, acetate, and propanoate at 0.1 M were reported to be 0.778, 0.778, 0.791, and 0.800, respectively (Robinson and Stokes, 1959). We also assume that all the organic anions used bear only one negative charge in our experimental conditions. This assumption is reasonable, since the corresponding acids have pK_a values <5 and are completely (>99.6%) ionized at pH 7.4. Glutamate bears two negatively and one positively charged group; the total charge calculated using reported ionization constants (Robinson and Stokes, 1959) is −1.002 at pH 7.4.

Ionic conductivities ($\chi(X)$) were calculated from the conductivities ($\chi(NaX)$) of solutions used for selectivity measurements as

$$\chi(X) = \chi(NaX) - \chi(b) - [\chi(NaCl)t_+], \quad (5)$$

where $\chi(b)$ is the conductivity of 5 mM HEPES-NaOH buffer (0.140 ± 0.001 mS/cm, $n = 5$); $\chi(NaCl)$ is the conductivity of 150 mM NaCl solution

(14.98 ± 0.02 mS/cm, $n = 5$); and t_+ is the cation transference number for 150 mM NaCl ($t_+ = 0.3838$, from Robinson and Stokes, 1959).

The hydrodynamic radii of PEG in Ringer solution were calculated from viscosity measurements at 25°C, as described previously (Sabirov et al., 1991; 1993). The Einstein's equation for spherical particles was used in the form

$$\eta_{sp} = [(2.5N_A 4/3\pi R_h^3)/1000]C, \quad (6)$$

where η_{sp} is the specific viscosity of polymer solution, N_A is Avogadro's number, C is the molar concentration of PEGs, and R_h is the hydrodynamic radius in centimeters. To account for the nonlinearity of concentration-dependence of viscosity of polymer solutions, R_h was determined for several concentrations, and the value was extrapolated to $C = 0$. The values for radii obtained in Ringer solution in the present study (see Table 2) were close (although not identical) to the values reported previously for 100 mM KCl solutions (Sabirov et al., 1991; 1993) and the values obtained by size exclusion chromatography (Kuga, 1981).

The dimensions of ATP^{4-} and $MgATP^{2-}$ were calculated using Molecular Modeling Pro computer software (Norgwyn Montgomery Software, North Wales, PA).

Data were analyzed in Origin 5.0 and Origin 6.0 (OriginLab, Northampton, MA). Pooled data are given as mean ± SE of observations (n). Where no error bar is shown, the mean ± SE value was smaller than the size of the symbol. Throughout, a weighted linear fit was used to generate fitting parameters and their standard errors. Statistical differences in slope conductances were evaluated by analysis of covariance using StatsDirect statistical software (StatsDirect, Cheshire, UK) and considered significant at $p < 0.05$.

RESULTS

Large organic anions move freely inside the maxi-anion channel pore

We first conducted selectivity experiments under bi-ionic conditions, omitting all components from both pipette and bath solutions except for NaCl and HEPES buffer, to unambiguously determine the permeability of maxi-anion channels to large organic anions. When the pipette was filled with the NaCl-HEPES solution, maxi-anion channels could be activated upon patch excision in the control Ringer bath solution. The channels remained active after replacing the control Ringer bath solution with the NaCl-HEPES solution. Therefore, extracellular divalent cations are not essential for channel activity. The channels were active at small applied voltages and inactivated when the membrane potential exceeded ±20 mV (Fig. 1 *A*). The I–V relationship under the above experimental conditions was linear and symmetrical with a reversal potential at 0 mV and a slope conductance of 403.9 ± 1.7 pS (Fig. 1 *B*). These values are close to those reported previously (Sabirov et al., 2001).

When NaCl in the bath solution was replaced with the sodium salts of formic, propanoic or lactobionic acids, the unitary I–V curves shifted to more negative potentials and became nonlinear (Fig. 1, *C–E*). We therefore fitted these curves with a polynomial (Eq. 1) and used the fitting parameters to calculate the reversal potentials (Eqs. 2 and 3). The I–V curves in Fig. 1 indicate a permeability sequence of *chloride* > *formate* > *propanoate* > *lactobionate*. The I–V relationships for other anions tested had intermediate reversal potentials, as summarized in Table 1. Permeability ratios (P_X/P_{Cl}) for different anions were calculated from the Goldman-Hodgkin-Katz equation for bi-ionic conditions (Eq. 4) and are collectively presented in Table 1.

The dependence of the permeability ratio on the ionic radius of organic anions (Fig. 2 *A*) reveals an important difference relative to other chloride channels. Although in most channels (both cation- and anion-selective) the permeability to ions cuts off at a certain ionic size (Hille,

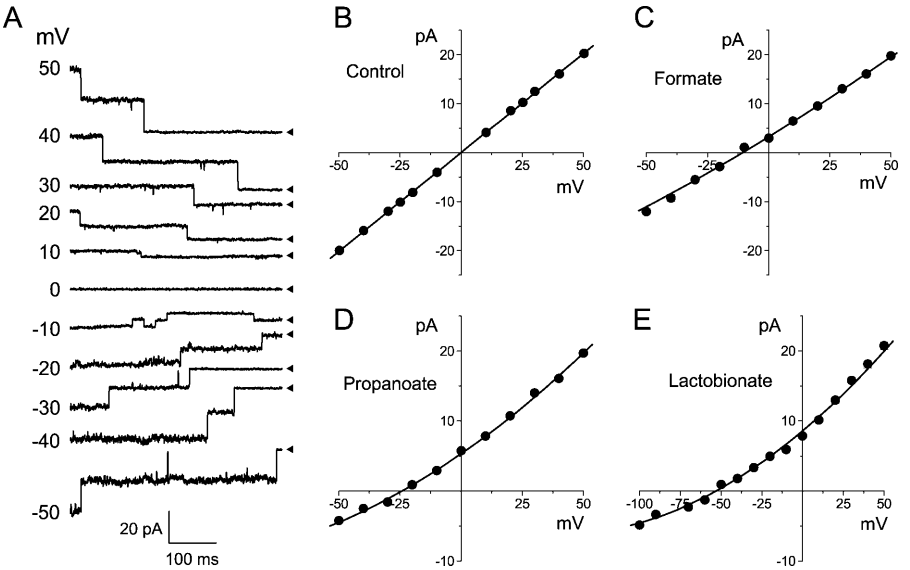

FIGURE 1 Single maxi-anion channel currents and I–V relationships in bi-ionic conditions. (*A*) Representative current traces recorded at different voltages from a patch containing two active channels. The pipette was filled with a solution containing 150 mM NaCl and 5 mM HEPES-NaOH (pH 7.4), and the maxi-anion channels were activated by excising the patch into control Ringer solution before challenging it with a solution of the same composition as that in the pipette. Arrowheads indicate the zero current level for each trace. (*B*) Unitary I–V relationship for the maxi-anion channel in symmetrical chloride conditions. Each data point represents the mean ± SE of 5–11 measurements from five different patches. The solid line is a linear fit with a slope conductance of 403.9 ± 1.7 pS. (*C–E*) Unitary I–V relationships for the maxi-anion channel recorded in asymmetrical conditions with 150 mM Cl^- in the pipette and 150 mM formate ($n = 5$–12), propanoate ($n = 5$–12), or lactobionate ($n = 4$–13) in the bath. Each data set was obtained from five different patches. The mean ± SE values are shown by vertical bars where the values exceed the symbol size. Solid lines are polynomial fits (Eq. 1). Reversal potentials calculated from Eq. 3 are −10.6 ± 0.6 mV, −24.1 ± 0.8 mV, and −53.0 ± 1.3 mV for formate, propanoate, and lactobionate, respectively.

TABLE 1 Selectivity of maxi-anion channel for different organic anions and ionic conductivity ratios

Anion	R_X (nm)	E_{rev} (mV)	P_X/P_{Cl}	$\chi(X)/\chi(Cl)$
Formate	0.212	−10.6 ± 0.6	0.662 ± 0.014	0.619 ± 0.003
Acetate	0.242	−17.7 ± 1.4	0.502 ± 0.027	0.450 ± 0.003
Propanoate	0.267	−24.1 ± 0.8	0.391 ± 0.011	0.378 ± 0.002
Glutamate	0.345	−46.9 ± 1.3	0.161 ± 0.008	0.266 ± 0.003
Pyruvate	0.271	−16.9 ± 1.7	0.518 ± 0.013	0.428 ± 0.003
Methanesulfonate	0.267	−17.5 ± 0.4	0.506 ± 0.009	0.508 ± 0.002
Gluconate	0.349	−45.9 ± 0.8	0.168 ± 0.005	0.198 ± 0.002
Glucuronate	0.363	−39.7 ± 1.6	0.190 ± 0.013	0.198 ± 0.002
Glucoheptonate	0.393	−40.7 ± 1.4	0.178 ± 0.013	0.153 ± 0.003
Lactobionate	0.487	−53.0 ± 1.3	0.127 ± 0.006	0.094 ± 0.002

R_X is the unhydrated radius calculated as a geometric mean of three dimensions according to the formula $R_X = (1/2)\,(l_1\, l_2\, l_3)^{1/3}$, where l_1, l_2, and l_3 are ion dimensions estimated from space-filling models (data were taken from Linsdell and Hanrahan, 1998). For E_{rev} determination, the unitary channel amplitudes were collected at different voltages from at least five different patches, the I–V curves were constructed, and reversal potentials were calculated from polynomial fits (Eqs. 1–3). Ionic conductivities $\chi(X)$ were calculated from experimentally measured solution conductivities, as described in Materials and Methods. Each value represents the mean ± SE of five observations.

2001), the maxi-anion channel was moderately permeable to all anions tested. Although the relative permeability decreased as the ionic radius increased, the channel remained permeable even to the largest anion tested, lactobionate. Therefore, it appears that the maxi-anion channel pore has a radius >0.487 nm, the size of lactobionate.

The minimum pore diameter can be estimated using the excluded area theory (Dwyer et al., 1980), which is based on the principle that the permeability is proportional to the cross-sectional area of the selectivity filter (the most constricted part of the pore),

$$P_X/P_{Cl} = k[1 - R_X/R_P]^2, \quad (7)$$

where R_X is the unhydrated radius of the organic anion; R_p is the radius of the pore; and k is a proportionality constant. Taking into account the friction force gives (Dwyer et al., 1980; Nilius et al., 1999)

$$P_X/P_{Cl} = (k/R_X)[1 - R_X/R_P]^2. \quad (8)$$

Fitting the permeability ratio data to these equations (Fig. 2 *A*) yielded estimates of 0.55 ± 0.04 nm (Eq. 7) and 0.75 ± 0.11 nm (Eq. 8) for the minimum pore radius.

The above treatment is valid only if the lower permeability for larger anions is due to the excluded volume effect when the anion size is close to the size of the pore. However, does the maxi-anion channel pore actually obstruct the movement of the organic anions tested? Assuming that ions move inside the pore by free diffusion without any interaction with the pore wall, we would expect that ionic selectivity would simply follow the ionic mobility. To what extent can the ionic permeability of the maxi-anion channel be attributed to the differences in ionic mobility? To answer this question, we used the ionic conductivities (see Eq. 5 and Table 1) as a measure of ionic mobility in our experimental solutions. Ionic conductivity ratios were surprisingly close to the permeability ratios for all anions tested (Table 1 and Fig. 2 *A*, *open circles*). Regression analysis revealed a strong correlation between the permeability ratio obtained by patch-clamp and the ionic conductivity ratio, with a correlation coefficient of 0.96 and a slope of 1.03 ± 0.11 (Fig. 2 *B*). This result strongly suggests that all organic anions tested, including bulky lactobionate, move freely inside the maxi-anion channel lumen without interference by the wall of the channel pore. Therefore, the value for the minimum pore radius obtained by this method appears to be an underestimate.

Small-sized polyethylene glycols reduce the unitary maxi-anion channel conductance

Since the size of the maxi-anion channel pore is likely to be larger than the size of lactobionate, the bulkiest anion tested, we sought an alternative way to estimate the dimensions of the channel. Noncharged polymeric polyethylene glycols have been employed for pore sizing experiments in planar lipid bilayers (for reviews see Krasilnikov, 2002; Bezrukov and Kasianowicz, 2002) but have never been used in patch-

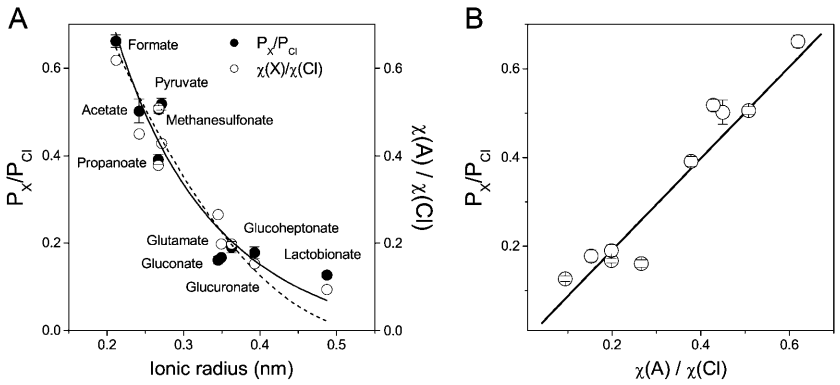

FIGURE 2 Ionic selectivity of the maxi-anion channel. (*A*) Solid circles represent the permeability ratios derived from bi-ionic potentials. Open circles represent ratios of ionic conductivities for the same anions in the bath solution, calculated from Eq. 5 (see Materials and Methods). The dashed line is a fit to Eq. 7 with k = 1.71 ± 0.25 and R_P = 0.55 ± 0.04 nm. The solid line is a fit to Eq. 8 with k = 0.28 ± 0.05 and R_P = 0.75 ± 0.11 nm. (*B*) Linear correlation between permeability ratios and ionic conductivity ratios for different organic anions. The slope is 1.03 ± 0.11, and the correlation coefficient R = 0.96 at $p < 0.0001$.

clamp experiments. When the polymer-containing solutions were infused into the bath after preactivation of maxi-anion channels (by patch excision under isotonic conditions with control Ringer solution in both the bath and pipette), it was found that most patch membranes were quickly destroyed. However, some membrane patches (particularly smaller ones made with 3–5 MΩ pipettes) survived for a longer time (up to 10–20 min). Examples of recordings made with such patches are shown in Fig. 3 *A*. Infusion of a small polymer, PEG 200 ($R_h = 0.455$ nm), to the bath suppressed the inward current through single maxi-anion channels (Fig. 3 *A*, *center panel*). Since the inward current corresponds to the outward flow of anions, we conclude that polymer molecules interfere with the entrance of ions to the inner mouth of the maxi-anion channel pore. In contrast, a large polymeric molecule, PEG 4000 ($R_h = 1.91$ nm), did not have such an effect on the unitary channel amplitude (Fig. 3 *A*, *right panel*). The slope for inward currents was decreased in the presence of PEG 200, whereas it was practically unchanged in the presence of PEG 4000 (Fig. 3 *B*). Intracellular application of PEGs slightly shifted the reversal potentials to more negative values (up to −5 mV). This could not be interpreted as a streaming potential, however, since we observed a similar shift using a pipette filled with 3 M KCl and without any membrane patch (data not shown), indicating that the shift might be due to a slightly altered bath electrode potential. For further analysis of the effects of polymers, we chose to use slope conductances calculated separately for inward and outward unitary currents rather than channel amplitudes at a fixed voltage to avoid the problem of reversal potential shift.

Outside application of the polymers could not be achieved in the outside-out configuration, because outside-out membrane patches were immediately destroyed upon perfusion of polymer containing solution. However, the polymers could be applied from the pipette solution in the cell-attached configuration. When pipettes were filled with control Ringer solution containing 20% (wt/vol) PEGs with a molecular weight of 200 or more, gigaOhm seal formation was not disrupted, and membrane patches survived for >5 min. Examples of recordings from such experiments are shown in Fig. 4 *A* (*left panel*). In this configuration, outward currents were predominantly suppressed by extracellular PEG 200, indicating that the polymer was now interfering with the anionic flux at the external mouth of the channel pore. Subsequent infusion of PEG molecules into the bath created a symmetrical configuration with polymer on both sides of the membrane patch, which was rather stable under this condition. With PEG 200 present on both sides of membrane, the channel currents decreased further (Fig. 4 *A*, *center panel*) and unitary I–V relationships became symmetrical (Fig. 4 *B*, *center panel*). PEG 4000 molecules failed to cause any inhibition of maxi-anion channel currents (Fig. 4, *A* and *B*, *right panels*).

Fig. 5 summarizes relative changes in the single-channel conductance of the maxi-anion channel due to the addition of PEGs and compares them with relative changes in the bulk conductivity due to PEGs. As shown in Fig. 5 *A*, PEG 200 added from the intracellular side alone had a profound suppressive effect on the inward conductance (chloride efflux). In contrast, the outward conductance (chloride influx) was more markedly suppressed than the inward conductance

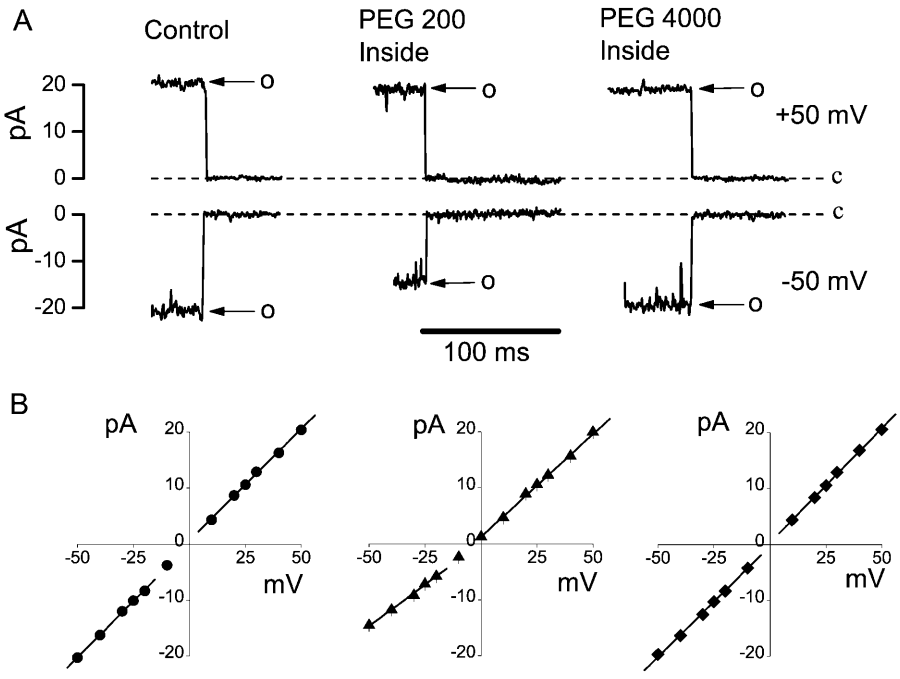

FIGURE 3 Effects of PEGs added only from the intracellular side on single maxi-anion channel currents. (*A*) Representative single-channel events recorded in the absence (*left panel*) and in the presence of PEG 200 (*middle panel*) or PEG 4000 (*right panel*) in the bath. Pipettes were filled with control Ringer solution, and the maxi-anion channels were activated by excising the patch into the control Ringer solution before challenging it with the test polymer-containing solution. (*B*) Current-voltage relationships for the maxi-anion channel in control symmetrical control Ringer solution (*left panel*) and with PEG 200 (*middle panel*) or PEG 4000 (*right panel*) present in the bath. Each symbol represents the mean value of 5–20 observations obtained from at least five different patches. Solid lines are linear fits with slopes corresponding to the unitary inward conductances of 402.8 ± 8 pS, 297 ± 13 pS, 395.3 ± 6.1 pS, and outward conductances of 400 ± 8.0 pS, 366.8 ± 5.0 pS, and 409.0 ± 6.0 pS for control, PEG 200 and PEG 4000, respectively.

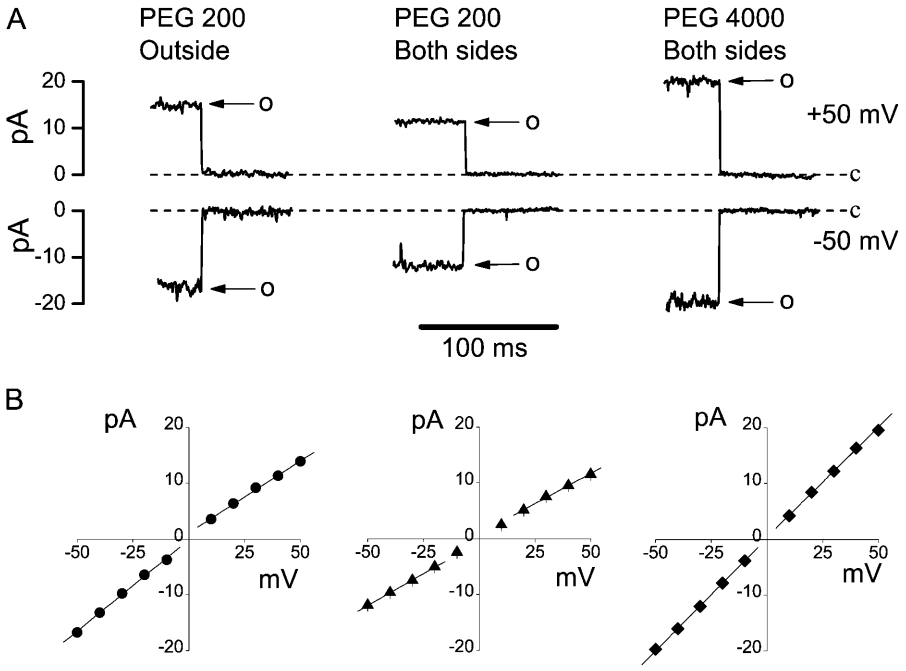

FIGURE 4 Effects of PEGs added from the extracellular side or both sides of the patch on single maxi-anion channel currents. (*A*) Representative single-channel events recorded when PEG 200 was added only to the pipette solution (*left panel*) and to both the pipette and bath solutions (*middle panel*), and when PEG 4000 was added to both the pipette and bath solutions (*right panel*). (*B*) Current-voltage relationships for the maxi-anion channel with PEG 200 present only in the pipette (*left panel*) and in both the pipette and bath (*middle panel*), and PEG 4000 present in both the pipette and the bath solution (*right panel*). Each symbol represents the mean of 5–19 observations obtained from at least five different patches. Solid lines are linear fits with slopes corresponding to the unitary inward conductances of 327.0 ± 9.7 pS, 227.5 ± 4.9 pS, and 404.5 ± 3.2 pS, and the outward conductances of 257.7 ± 5.8 pS, 216.8 ± 7.1 pS, and 395 ± 11 pS in the left, middle, and right panels, respectively.

when the same polymer was present only on the extracellular side of the membrane patch. Two-sided application of PEG 200 induced even more prominent suppression of both inward and outward conductances. Importantly, both inward and outward conductances were lowered to the same extent as the bulk conductivity of the control Ringer solution (Fig. 5 *B*). Our interpretation is that small PEG 200 polymers can freely access the interior of the maxi-anion channel pore and that the decrease in the unitary conductance is likely due to decreased ionic mobility in the presence of the PEGs (as estimated by conductivity measurements). Although the decrease in the bulk conductivity due to the presence of large PEG 4000 molecules was similar to that for PEG 200 (Fig. 5 *B*), the polymer failed to suppress the unitary current of the maxi-anion channel (Fig. 5 *A*). A straightforward interpretation of this failure is that the PEG 4000 molecule cannot access the channel interior because it is larger than the size of the pore entrance. Varying the molecular weight of the polymers should therefore allow accurate determination of the size of the maxi-anion channel pore.

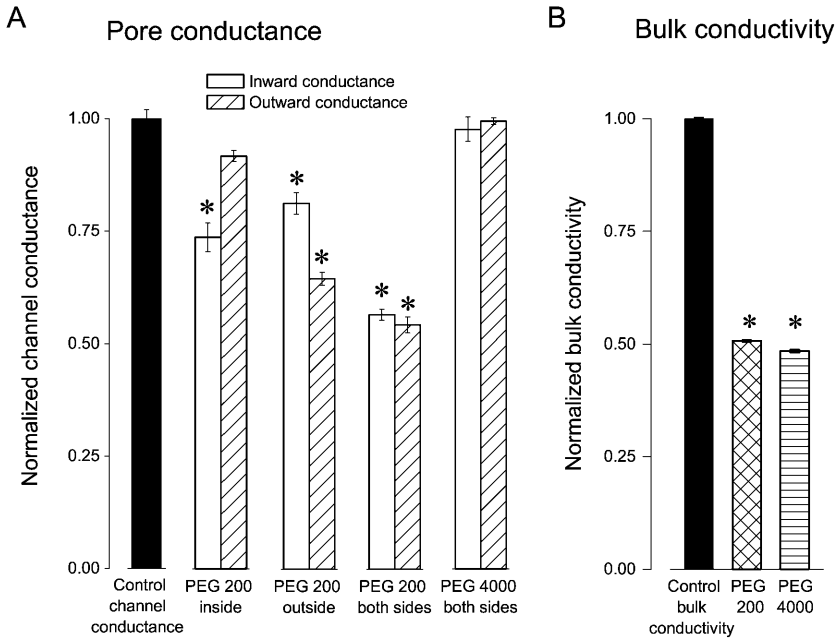

FIGURE 5 Effects of PEG 200 and PEG 4000 on unitary maxi-anion channel conductances and bulk solution conductivities. (*A*) Pore conductance changes by addition of PEG 200 and PEG 4000 from the inside, outside, and both sides of membrane patches. Open bars represent the inward conductance, and hatched bars the outward conductance. Asterisk symbol means significantly different from the control at $p < 0.05$. (*B*) Changes in bulk conductivity by addition of PEG 200 and PEG 4000. The electrical conductivity of control Ringer solution (control) was 15.24 ± 0.03 mS/cm ($n = 5$). Asterisk symbol means significantly different from the control at $p < 0.05$.

One-sided application of polymeric molecules reveals an asymmetry in maxi-anion channel entrances

We have tested all available PEGs with molecular weights in the range of 200–4000 as well as smaller molecules such as ethylene glycol and glycerol. Unitary maxi-anion channel conductances obtained with these polymers applied from only the inside or outside are summarized in Table 2. Membrane patches did not survive when ethylene glycol or glycerol was added to the pipette solution. Therefore, data could not be obtained for the outward conductance using these molecules.

All polymers tested efficiently decreased the bulk conductivity. However, the maxi-anion channel conductance was affected only by PEGs with molecular weights of up to 1540 when they were added from either side of the membrane. The degree to which channel amplitude was suppressed strongly depended on the sidedness of the polymer application. The inward conductance when PEG 1000 was applied from inside (369.2 ± 4.7 pS, $n = 5$) was close to the control value of 402.8 ± 5.1 pS ($n = 6$: $p = 0.002$), whereas the outward conductance with the same polymer in the pipette (274.9 ± 8.6 pS, $n = 5$) was still only slightly higher than the conductance with PEG 200 (257.7 ± 5.8 pS, $n = 5$: $p = 0.67$) present in the pipette. In Fig. 6, the relative effect of polymers added to either the intracellular or extracellular side is plotted as a function of the hydrodynamic radii of the polymers. The striking difference in the relative effect of the same polymers added from different sides of the membrane suggests that the entrances to the maxi-anion channel are asymmetrical.

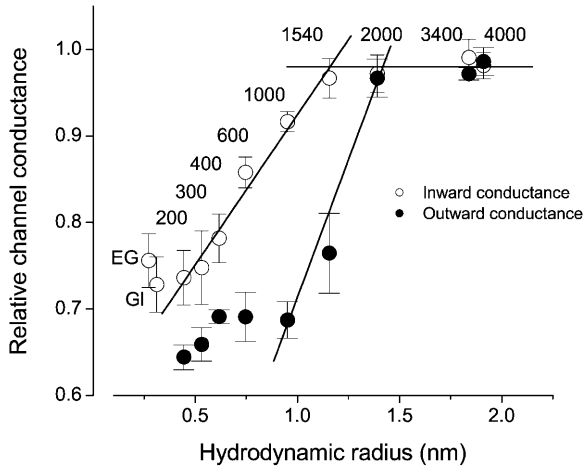

FIGURE 6 Relative changes in unitary maxi-anion single-channel conductances as a function of hydrodynamic radii (R) of nonelectrolyte polymer molecules upon one-sided application of polymer. Open circles represent the inward conductance of channel when polymers were added only to the bath solution. The ascending straight line on the left is a linear fit to the data points for PEG 200–PEG 1540. The point of the intersection with the plateau level is at $R = 1.16$ nm. Solid circles represent the outward conductance of channel when polymers were added only to the pipette solution; the ascending straight line on the right is a linear fit to the data points for PEG 1000–PEG 2000 and crosses the plateau level at $R = 1.42$ nm. *EG* represents ethylene glycol, and *Gl* is glycerol. Mean single-channel amplitudes at different voltages ($n = 5$–20 from at least five different patches) were used to construct I–V relationships and calculate slope conductances. Error bars represent standard errors of the linear fits.

TABLE 2 Single-channel conductances in the presence of polymer nonelectrolytes applied from one side

Nonelectrolyte	R_h (nm)	γ_{in} (pS)	γ_{out} (pS)	χ (mS/cm)
Control	—	402.8 ± 5.1	400.0 ± 8.0	15.24 ± 0.03
Ethylene glycol	0.272 ± 0.002	305 ± 13	—	8.66 ± 0.02
Glycerol	0.311 ± 0.002	293 ± 13	—	8.68 ± 0.04
PEG 200	0.445 ± 0.011	297 ± 13	257.7 ± 5.8	7.72 ± 0.02
PEG 300	0.532 ± 0.002	301 ± 17	263.6 ± 7.7	7.70 ± 0.02
PEG 400	0.617 ± 0.005	315 ± 11	276.5 ± 3.1	7.56 ± 0.03
PEG 600	0.746 ± 0.003	345.6 ± 7.2	276 ± 11	7.52 ± 0.02
PEG 1000	0.951 ± 0.010	369.2 ± 4.7	274.9 ± 8.6	7.51 ± 0.03
PEG 1540	1.156 ± 0.013	389.4 ± 9.2	306 ± 19	7.42 ± 0.02
PEG 2000	1.391 ± 0.006	391.6 ± 8.7	386.8 ± 8.8	7.44 ± 0.04
PEG 3400	1.839 ± 0.020	399.0 ± 8.5	388.8 ± 2.9	7.46 ± 0.03
PEG 4000	1.911 ± 0.005	395.3 ± 6.1	394.5 ± 6.4	7.38 ± 0.02

R_h is the hydrodynamic radius obtained from viscosity measurements; γ_{in} is the inward single-channel conductance in the presence of polymers applied from the intracellular side of membrane patches; γ_{out} is the outward conductance in the presence of polymers applied from the extracellular side of membrane patches; and χ is the solution conductivity in the absence (control) or presence of polymers. Mean single-channel amplitudes at different voltages ($n = 5$–20 from at least five different patches) were used to construct I–V relationships and calculate slope conductances and their standard errors. Each value for the bulk conductivity represents the mean ± SE of five observations.

Size-dependent effects of these nonelectrolytes on the maxi-anion channel conductance are apparent in the rising phase in Fig. 6 and correspond to the partitioning of nonelectrolytes between the channel interior and bulk solution. A size-independent plateau level was seen for larger PEGs and corresponds to complete exclusion of the nonelectrolytes from the channel lumen. An obvious way to estimate the pore size from these experiments would be to determine the cutoff size for the polymers, defining it as the point of intersection between the rising phase and the upper plateau level. The two lines crossed at 1.16 nm for intracellular, and at 1.42 nm for extracellular application of nonelectrolytes. Thus, the channel entrance facing the extracellular environment is slightly wider than the entrance facing the intracellular compartment.

In these experiments, when nonelectrolytes were added to only one side, even the smallest molecules tested did not fully suppress the single-channel conductance to the level of the bulk solution conductivity (Fig. 6), suggesting only partial partitioning. This could be due to constant outflow of nonelectrolyte molecules from the opposite mouth of the channel. In addition, flux of the solvent driven by its chemical potential gradient (toward the nonelectrolyte-containing side) would also reduce the nonelectrolyte

concentration inside the pore and decrease its partitioning. Local changes in Cl^- concentration due to osmotic water flow may also affect the results presented, although this effect is probably minimal, since in the presence of nonpenetrating large molecules the channel conductance was close to the control level measured in nonelectrolyte-free conditions.

Two-sided application of polymeric molecules yields an average pore size for the maxi-anion channel

Polymeric nonelectrolytes were applied to both sides of a membrane patch excising the patch with a PEG-containing pipette and subsequently infusing the same polymer into the bath. In such two-sided experiments, the effect of polymers (Table 3 and Fig. 7) was more symmetrical than in one-sided experiments. In general, the outward unitary conductance was a little more sensitive to the presence of a polymer compared to the inward conductance. This difference was most profound for PEG 1000. In the presence of PEG 200 or 300, the ratio of the channel conductances in the presence and absence of PEG was similar to the ratio of bulk aqueous conductivities with and without polymer (Fig. 7), a fact suggesting that the ionic environment in the pore interior is almost identical to that in the bulk solution and is affected by small polymers in the same way. Size-dependent changes in the channel conductance observed with PEG 400–1540 would represent partial access of the polymers to the channel interior, and the upper plateau would represent complete exclusion of large polymers from the channel lumen. The bulk solution conductivity, on the other hand, decreased when polymer was present but was almost insensitive to the polymer molecular weight and hence, the polymer size.

Straight lines fitted to the data points of the rising phase crossed the upper plateau level at 1.28 nm for the inward conductance and 1.34 nm for the outward conductance (Fig. 7). These values are close to each other and intermediate to those derived from the one-sided experiments (Fig. 6).

TABLE 3 Single-channel amplitudes in the presence of PEGs applied from both sides of membrane patch

Polymer	γ_{in} (pS)	γ_{out} (pS)
PEG 200	227.5 ± 4.9	216.8 ± 7.1
PEG 300	225.5 ± 3.9	222.6 ± 4.4
PEG 400	243.4 ± 1.5	233.3 ± 3.8
PEG 600	274.4 ± 5.4	261.7 ± 5.6
PEG 1000	323.5 ± 5.0	284.7 ± 3.0
PEG 1540	365.2 ± 3.9	351.8 ± 2.3
PEG 2000	390.9 ± 3.9	390.2 ± 7.7
PEG 3400	391.6 ± 6.0	383.6 ± 7.1
PEG 4000	404.5 ± 3.2	395 ± 11

γ_{in} and γ_{out} are the inward and outward conductances, respectively. The unitary channel amplitudes (n = 5–20) were collected at different voltages from at least five different patches, the I–V curves were constructed, and the slope conductances and their standard errors were obtained from linear fits at positive and negative potentials.

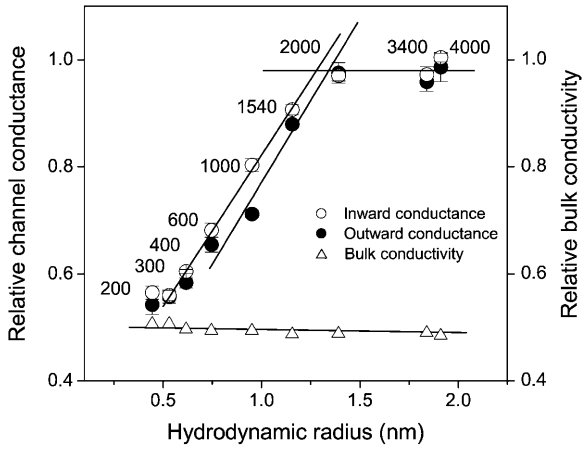

FIGURE 7 Relative changes in unitary maxi-anion single-channel conductances as a function of the hydrodynamic radii (R) of nonelectrolyte polymer molecules applied from both sides of membrane patches. The ascending straight line for channel inward conductances (*open circles*) is a linear fit to the data points for PEG 300–PEG 1540 and crosses the plateau level at R = 1.28 nm. The ascending straight line for outward conductances (*solid circles*) is a linear fit to the data points for PEG 600–PEG 2000 and crosses the plateau level at R = 1.34 nm. Relative decreases in the bulk conductivity of the polymer-containing control Ringer solutions used in these experiments (*open triangles*) are also plotted. Mean single-channel amplitudes at different voltages (n = 5–20 from at least five different patches) were used to construct I–V relationships and calculate slope conductances. Error bars represent standard errors of the linear fits.

Normalizing the change in channel conductance by the change in bulk solution conductivity allows the derivation of a parameter (ν), which was initially interpreted as a permeability parameter (Sabirov et al., 1991; 1993; Krasilnikov et al., 1992) and was later reinterpreted as a partition coefficient (Bezrukov et al., 1996; Rostovtseva et al., 2002b),

$$\nu = [(\gamma - \gamma_O)/\gamma_O]/[(\chi - \chi_O)/\chi_O], \quad (9)$$

where γ and χ are the channel conductance and bulk solution conductivity, respectively, in the presence of nonelectrolytes, γ_O and χ_O are the same parameters in control Ringer solution that does not contain nonelectrolytes. Partition coefficients for all PEG molecules used are plotted in Fig. 8 as a function of polymer hydrodynamic radius. In these plots, the descending portion of the curve corresponds to a zone of transition from full penetration to complete exclusion. The pore cutoff size was obtained by determining the point of intersection of straight lines fitted to the data points of descending part of the curve and the lower plateau level. The cutoff sizes determined using the inward and outward conductances were 1.29 nm and 1.38 nm, respectively. These values are close to those derived from the analysis of relative channel conductance changes.

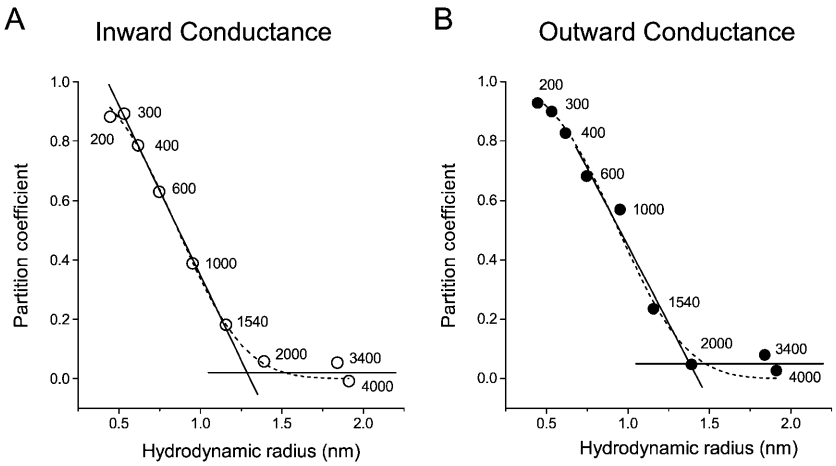

FIGURE 8 Partitioning of PEGs into the maxi-anion channel pore. Partition coefficients for inward (*A*) and outward (*B*) unitary conductances were calculated according to Eq. 9 and plotted as a function of the polymer hydrodynamic radius (R). The solid descending line for the inward conductance is a linear fit to the data points for PEG 300–PEG 1540. The point of intersection with the lower plateau is at $R = 1.29$ nm. The solid straight descending line for the outward conductance is a linear fit to the data points for PEG 600–PEG 2000. The crossing point with the lower plateau is at $R = 1.38$ nm. The dashed lines are fits to Eq. 10 with $R_p = 0.97 \pm 0.02$ nm and $\alpha = 3.07 \pm 0.17$ for the inward conductance and $R_p = 1.06 \pm 0.03$ nm and $\alpha = 3.27 \pm 0.33$ for the outward conductance (see text for details).

An alternative way of analyzing the nonelectrolyte partitioning is to fit the data to a scaling law of the form (Bezrukov et al., 1996; Merzlyak et al., 1999; Rostovtseva et al., 2002b)

$$\nu = \exp[-(R_N/R_p)^{\alpha}], \tag{10}$$

where R_N and R_p are the radius of nonelectrolyte (PEG) and pore, respectively, and α characterizes the sharpness of the transition between regimes of exclusion and penetration. Fitting our experimental curves (Fig. 8, *dashed lines*) yielded $R_p = 0.97 \pm 0.02$ nm using the inward conductance and $R_p = 1.06 \pm 0.03$ nm using the outward conductance. These values are smaller than the pore size empirically obtained by determining the cutoff size for polymers that can enter the channel. The reason for this is that R_p corresponds to the size of a PEG with $\nu = 0.38$ (when $R_N = R_p$ in Eq. 10). Such a molecule would only be partially excluded from the channel; however, the size obtained by determining the cutoff size corresponds to the point where no partitioning, or full exclusion, is observed (plateau level at $\nu \sim 0$). We therefore believe that this fitting underestimates the actual size of channel pore.

DISCUSSION

Voltage-gated Na^+, K^+, and Ca^{2+} channels in excitable membranes are highly selective for Na^+, K^+, and Ca^{2+} (Hille, 2001). Some anion channels, however, are promiscuous and pass not only the title anion (chloride for Cl^- channels) but also other negatively charged particles mediating the release of these substances from cells. The volume-sensitive outwardly rectifying (VSOR) anion channel is one such channel and its permeability to amino acids (such as taurine) is as important as its chloride permeability (Strange et al., 1996; Okada, 1997). Another example is the maxi-anion channel which has been suggested to serve as a conductive pathway for ATP release in mouse mammary C127 cells (Sabirov et al., 2001; Dutta et al., 2002) and *macula densa* cells (Bell et al., 2003). Fixed charges and dipoles could create a favorable electrostatic environment in the pathway of the permeating ion, allowing its effective transport. However, even with the proper electrostatic profile, the channel could hardly pass amino acids and other organic metabolites unless it had a pore of sufficient size. The ion channel pore size is therefore a key structural determinant of permeability to physiologically meaningful cytosolic components. Either charged or uncharged molecules of variable size can be used as a probe to assess the size of the channel pore.

Permeation of large organic anions through the maxi-anion channel

Permeability to large organic ions is most frequently used for assessment of the pore size of ion channels (Hille, 2001). In most cases such experiments reveal a cutoff size, which is interpreted as an estimate for the minimum size of the channel pore. In our experiments, the permeability of the maxi-anion channel gradually decreased as the ionic radius increased, although the channel remained permeable even to the largest test anion, lactobionate. The interpretation of permeability data may depend on the theoretical mechanism of ionic transport through the channel under consideration. If we assume a free diffusion of hydrated ions inside the pore, we should expect the permeability to be affected by the ionic mobility. For the maxi-anion channel, we found a linear relationship between permeability ratios and ionic mobility ratios (measured as the ratio of ionic conductances) with a slope close to 1. This result suggests that ions (even the bulkiest organic anions used in our experiments) move inside the maxi-anion channel by free diffusion with little or no interference by the channel wall. Based on this, we consider even the upper estimate of 0.75 nm for the minimum pore radius derived in these experiments using the excluded area theory (Dwyer et al., 1980) to be an underestimate of the

maxi-anion channel pore size. Soejima and Kokubun (1988) estimated the cross-sectional size of maxi-anion channels in cultured smooth muscle cells to be at least 32 $Å^2$ (corresponding to a pore radius of 0.32 nm). This figure was derived from the authors' estimation of the ionic dimensions of HEPES, the permeability of which could not be detected. We believe that this value is also an underestimate for the same reasons.

Pore sizing by nonelectrolyte size-exclusion method

Nonelectrolytes have an obvious advantage as probes for pore sizing, in that they are relatively inert with respect to the electrostatics which govern the movement of ions in channel pores. However, to measure net nonelectrolyte fluxes, radiolabeled tracers must be employed, and this technique is useful only for determining the macroscopic membrane permeability (Finkelstein, 1987), not the permeability at the single-channel level. Krasilnikov et al. (1988) first noticed that PEGs of different molecular weights had differential effects on the current amplitude of ion channels formed by *Staphylococcus aureus* α-hemolysin in lipid bilayers: only PEGs with a molecular weight <3000 suppressed the channel amplitude, whereas larger molecules had no effect despite their ability to decrease the bulk conductivity. Sabirov et al. (1991, 1993) and Krasilnikov et al. (1992) studied the ionic conductivity and viscosity of polymer-containing solutions and their effects on single-channel amplitudes using planar lipid bilayers, and concluded that PEGs can be used to accurately determine the pore size of ion channels. The method has been widely used to estimate the pore size of channels in lipid bilayer experiments and has yielded pore dimensions consistent with x-ray crystallography data for staphylococcal α-hemolysin (Merzlyak et al., 1999) and bacterial porin OmpF (Rostovtseva et al., 2002b), and electron microscopy data for mitochondrial porin VDAC (Krasilnikov et al., 1996; Carneiro et al., 1997; 2003).

The most attractive feature of the nonelectrolyte partitioning method is that it permits testing nonelectrolyte size-exclusion at the single-channel level. PEGs are inert linear polymers, which obey the viscosity law for random coils in water solutions (Sabirov et al., 1991, 1993) and are widely used as tools for pore-sizing experiments (Krasilnikov, 2002; Bezrukov and Kasianowicz, 2002). The necessity of employing high concentrations of nonelectrolytes, however, has restricted the use of this method to lipid bilayers. The present study is the first attempt to assess channel pore size by using this approach in patch-clamp experiments. To our surprise, osmotic gradients that developed upon administration of nonelectrolytes from either side did not prevent the formation of gigaOhm contacts. Although the stability of membrane patches was greatly decreased, the patches survived long enough to allow accurate measurements of channel activity. When osmotic symmetry was restored by introducing polymer to both sides, membrane patches regained their stability, although the membrane patches were still considerably less stable than in control nonelectrolyte-free conditions. We thus conclude that, with some effort, the nonelectrolyte size-exclusion method can be adopted for use in conventional patch-clamp experiments for ion channel pore sizing.

Although a simple interpretation of the nonelectrolyte size-exclusion data given in the present article seems reasonable, the mechanism of polymer partitioning into nanoscale pores is far from being understood in detail. The hard sphere partitioning theory appears to be more adequate than a scaling approach based on the difference in entropy of a flexible polymer chain partitioned between the bulk solution and cylindrical pore (Bezrukov et al., 1996; Bezrukov and Kasianowicz, 1997, 2002; Merzlyak et al., 1999; Rostovtseva et al., 2002b). However, when sulfhydryl-directed PEG reagents were used to probe the pore of genetically engineered staphylococcal α-hemolysin ion channels at low concentrations, polymer partitioning (that determines the rate of irreversible modification of the cysteine residue projected into the lumen) did obey the scaling law (Movileanu and Bayley, 2001; Movileanu et al., 2003). Therefore, it is possible that the mechanism of polymer partitioning differs depending on the concentration of the polymer used, because of a shift from the diluted to the semidiluted regime of polymer-polymer interactions. The interaction of polymers with the α-hemolysin channel pore seems to be complex, as high-resolution recordings using unmodified PEGs revealed short (85% of total) and long (15% of total) blocking events; only long events obeyed the scaling law, whereas partitioning calculated from short events as well as their overall partition coefficients displayed somewhat steeper dependence on polymer mass (Movileanu et al., 2003). The dependence of PEG partitioning on pH (Bezrukov and Kasianowicz, 1997) adds even more complexity to the mechanism of the phenomenon, suggesting importance of hydration state of the channel pore.

Pore size of maxi-anion channel suits its function as an ATP channel

Adenosine 5′-triphosphate has a rigid adenosine core and rather flexible triphosphate tail. In crystals, this tail is seen to be folded back toward the adenine base, for both the Na-salt form of ATP (Kennard et al., 1971) and the Mg^{2+}-complexed form (Cini et al., 1984). After energy minimization using the MM2 algorithm of Molecular Modeling Pro computer software (see Materials and Methods), we obtained a similar conformation for ATP^{4-} and calculated the effective radius (as a geometric mean of three dimensions; see Table 1 legend for formula) to be 0.57–0.58 nm. The nonenergy-minimized conformation of ATP^{4-} with a stretched-out triphosphate had an effective radius of 0.57–0.65 nm depending on the directions of the three

dimensions. Rostovtseva and Bezrukov (1998) obtained a value of 0.77 nm by making conductivity measurements of ATP-containing solutions, considering the ATP^{4-} anion as a nonconducting particle. Even the conventional organic anion permeability method applied to maxi-anion channels gave an estimate of minimal pore size (0.75 nm) comparable to the size of ATP^{4-}. The size of ATP^{4-} corresponds to the hydrodynamic radius of PEG 400–600. Both PEG 400 and PEG 600 greatly altered the single-channel conductance of the maxi-anion channel in all experimental conditions used in our study, namely, during one-sided application of PEG from the extracellular or intracellular side (Fig. 6) and during symmetrical two-sided application of polymer (Fig. 7). This result suggests that PEG 400 and PEG 600 penetrate the pore of the maxi-anion channel. Therefore, the maxi-anion channel pore is accessible to particles the size of ATP^{4-}. The PEG cutoff radius for the maxi-anion channel pore was in the range of 1.2 nm to 1.4 nm. This range of values is considerably larger than the size of ATP^{4-}. Thus, we conclude that the maxi-anion channel pore provides sufficient room for accommodation and passage of ATP^{4-} and that the size of the pore perfectly fits with the proposed physiological function of maxi-anion channel as an ATP release channel. A weak ATP-binding site in the middle of the maxi-anion channel pore, which was revealed by voltage-dependent open-channel block by ATP^{4-}, is accessible from both sides of the channel and is designed to facilitate the electrodiffusional translocation of ATP, which could be detected as an ATP current (Sabirov et al., 2001). Rostovtseva et al. (2002a) have recently demonstrated that mitochondrial VDAC channel can select among polyanions of similar size but with different shape and charge distribution. Thus, proper dimensions of the channel pore should be considered as a necessary but not sufficient condition for ion permeation, and an intrinsic ATP-binding site may provide a favorable environment for the effective transport of ATP.

In the presence of Mg^{2+}, ATP^{4-} forms a stable 1:1 complex with the metal ion bound to the γ- and β-phosphates, but not to the nitrogen atoms of the adenine base (Cini et al., 1984; Sigel, 1987). We modeled $MgATP^{2-}$ with magnesium bound to either the β- or γ-phosphate and obtained an effective radius of 0.59–0.61 nm, which is only slightly larger than the effective radius of ATP^{4-}. Using the same method as was previously described for ATP^{4-} permeability (Sabirov et al., 2001), we obtained a P_{MgATP}/P_{Cl} of 0.127 (R. Z. Sabirov and Y. Okada, unpublished observation). Thus, the maxi-anion channel possesses a pore suitable not only for ATP conduction but also for physiologically important electrogenic $MgATP^{2-}$ transport.

Even a highly ATP-permeable pore would be ineffective if closed under physiological conditions due to voltage-dependent gating. The maxi-anion channel closes at high positive and negative voltages. However, at the membrane potential of -50 to -30 mV (typical for nonexcitable ATP-releasing cells), the open probability of maxi-anion channel is 0.1–0.8 (Sabirov et al., 2001). Therefore, the channel may spend a sufficient time in the open state to provide a physiologically relevant amount of released ATP.

Molecular identity of maxi-anion channel: the maxi-anion channel = pl-VDAC hypothesis

Maxi-anion channels have been observed in a wide variety of cell types (Strange et al., 1996), suggesting their general physiological role. Biophysical properties, such as the large unitary conductance and bell-shaped voltage dependency of maxi-anion channel gating in C127 cells, are similar to those of the voltage-dependent anion channel (VDAC) expressed in the outer membrane of mitochondria (Schein et al., 1976; Colombini, 1979; Wunder and Colombini, 1991). Buettner et al. (2000) identified an alternative first exon in the murine *vdac-1* gene that leads to the expression of an alternative form of porin with a leader peptide at its N-terminus which provides a signal targeting the protein to the plasma membrane through the Golgi apparatus; the signal peptide is eventually cleaved away to produce a plasmalemmal VDAC protein identical to the mitochondrial one. The VDAC protein is indeed found in the plasma membrane of various cells (Thinnes et al., 1989; Dermietzel et al., 1994; Jakob et al., 1995; Eben-Brunnen et al., 1998; Bathori et al., 1999; Buettner et al., 2000; Steinacker et al., 2000). It has been suggested that maxi-anion channels are formed by plasmalemmal VDAC (pl-VDAC) in rat astrocytes (Dermietzel et al., 1994), PC12 cells (Buettner et al., 2000), and C1300 neuroblastoma cells (Bahamonde and Valverde, 2003; Bahamonde et al., 2003).

Probing the mitochondrial porin by the nonelectrolyte partitioning method using conditions similar to those in our experiments with two-sided application of PEG yielded a value for the pore radius of 1.5 nm for the fully open state of the channel in lipid bilayers (Krasilnikov et al., 1996). This figure is very close to the cutoff size of $\sim$1.3 nm obtained in our experiments with the maxi-anion channel. Later, using the asymmetric PEG application method, Carneiro et al. (1997, 2003) described an asymmetrical pore for mitochondrial VDAC with radii of $\sim$1 nm and $\sim$2 nm for its *cis*- and *trans*-entrances, respectively (*cis* designates the side of the bilayer from which protein was added). This asymmetry parallels the asymmetry of maxi-anion channel entrance which was revealed by our experiments with one-sided application of PEG (Fig. 6). Electron microscopic images demonstrated that mitochondrial porin has an inner radius of $\sim$1.4 nm (Mannella, 1998), which is very close to the value obtained by polymer size exclusion for VDAC in lipid bilayers and for the maxi-anion channel in our patch-clamp study. Thus, the structural features of mitochondrial porin and the ATP-conductive maxi-anion channel do converge. Given that maxi-anion channels also resemble mitochondrial porins with respect to its open-channel block

by ATP (Rostovtseva and Bezrukov, 1998) and ATP permeability or conductivity (Rostovtseva and Colombini, 1997; Rostovtseva and Bezrukov, 1998; Rostovtseva et al., 2002a), it is tempting to conclude that the above hypothesis of maxi-anion and pl-VDAC identity is indeed valid. However, such similarities could be circumstantial and it will be necessary to reproduce the maxi-anion channel phenotype by heterologous expression of plasmalemmal VDAC gene in cells lacking maxi-anion channels. It will also be necessary to demonstrate that the permeation properties of the expressed channels are sensitive to site-directed mutagenesis.

Comparison with other candidate ATP-conductive anion channels

CFTR is under consideration as a candidate ATP release pathway (for recent reviews see Cantiello, 2001; Schwiebert and Zsembery, 2003; Sabirov and Okada, 2004). Linsdell et al. (1997) studied the permeability of the CFTR chloride channel to different anions and found the minimum functional pore diameter to be 0.53 nm (R_P ~0.27 nm). A similar result was obtained in Calu-3 cells with an endogenous CFTR conductance (Illek et al., 1999). However, CFTR displayed a strong ATP-hydrolysis-dependent asymmetry in permeation properties and allowed the passage of large organic anions (like lactobionate) added from the intracellular, but not from the extracellular, side with functional pore diameter of 1.38 nm (R_P ~0.69 nm) for kosmotropic organic anions (Linsdell and Hanrahan, 1998).

The volume-sensitive outwardly rectifying (VSOR) anion channel was also proposed to serve as an ATP-conductive pathway in aortic endothelial cells (Hisadome et al., 2002). The permeability of this channel to anions of different size yielded a pore diameter of 0.73 nm or 1.15 nm (R_P ~0.37–0.58 nm) depending on whether or not frictional forces were taken into account (Nilius et al., 1999). Droogmans et al. (1998, 1999) demonstrated that basket-shaped compounds, calixarenes, act as permeant blockers of VSOR channels, and found the lower and upper limits for the cross-sectional dimensions of the channel pore to be 1.1 × 1.2 nm and 1.7 × 1.2 nm, respectively. The pore radius calculated as a geometric mean of these dimensions is 0.57 nm and 0.71 nm, respectively.

Comparing these values with the results of our study, we conclude that the maxi-anion channel has the largest pore dimensions of all three candidate ATP-conducting pathways. This channel is therefore best-suited to its function as an ATP-conductive channel. However, the highest estimates for the pore size of the CFTR and VSOR chloride channels are comparable to the dimensions of the ATP^{4-} anion. Therefore, making a judgment based only on their pore sizes, we cannot completely rule out the hypothesis that these channels also take part in the regulated release of ATP under certain conditions.

The authors thank E.L. Lee for reviewing the manuscript, V.I. Ternovsky for helpful discussion, T. Okayasu for secretarial help, and M. Ohara and K. Shigemoto for technical support.

This work was supported by Grants-in-Aid for Scientific Research *A* and *C* to Y.O. and R.Z.S. from the Ministry of Education, Culture, Sports, Science and Technology of Japan.

REFERENCES

Abraham, E. H., A. G. Prat, L. Gerweck, T. Seneveratne, R. J. Arceci, R. Kramer, G. Guidotti, and H. F. Cantiello. 1993. The multidrug resistance (mdr1) gene product functions as an ATP channel. *Proc. Natl. Acad. Sci. USA.* 90:312–316.

Bahamonde, M. I., J. M. Fernandez-Fernandez, F. X. Guix, E. Vazquez, and M. A. Valverde. 2003. Plasma membrane voltage-dependent anion channel mediates anti-estrogen-activated maxi Cl^- currents in C1300 neuroblastoma cells. *J. Biol. Chem.* 278:33284–33289.

Bahamonde, M. I., and M. A. Valverde. 2003. Voltage-dependent anion channel localises to the plasma membrane and peripheral but not perinuclear mitochondria. *Pflugers Arch.* 446:309–313.

Bathori, G., I. Parolini, F. Tombola, I. Szabo, A. Messina, M. Oliva, V. De Pinto, M. Lisanti, M. Sargiacomo, and M. Zoratti. 1999. Porin is present in the plasma membrane where it is concentrated in caveolae and caveolae-related domains. *J. Biol. Chem.* 274:29607–29612.

Bell, P. D., J. Y. Lapointe, R. Sabirov, S. Hayashi, J. Peti-Peterdi, K. Manabe, G. Kovacs, and Y. Okada. 2003. *Macula densa* cell signaling involves ATP release through a maxi anion channel. *Proc. Natl. Acad. Sci. USA.* 100:4322–4327.

Bezrukov, S. M., and J. J. Kasianowicz. 1997. The charge state of an ion channel controls neutral polymer entry into its pore. *Eur. Biophys. J.* 26:471–476.

Bezrukov, S., and J. J. Kasianowicz. 2002. Dynamic partitioning of neutral polymers into a single ion channel. *In* Structure and Dynamics of Confined Polymers. J. J. Kasianowicz, M. S. Z. Kellernayer, and D. W. Deamer, editors. Kluwer, Dordrecht, The Netherlands. 93–106.

Bezrukov, S., I. Vodyanoy, R. Brutyan, and J. J. Kasianowicz. 1996. Dynamics and free energy of polymers partitioning into a nanoscale pore. *Macromolecules.* 29:8517–8522.

Bodas, E., J. Aleu, G. Pujol, M. Martin-Satue, J. Marsal, and C. Solsona. 2000. ATP crossing the cell plasma membrane generates an ionic current in *Xenopus* oocytes. *J. Biol. Chem.* 275:20268–20273.

Bosch, I., G. R. Jackson, Jr., J. M. Croop, and H. F. Cantiello. 1996. Expression of *Drosophila melanogaster* P-glycoproteins is associated with ATP channel activity. *Am. J. Physiol.* 271:C1527–C1538.

Buettner, R., G. Papoutsoglou, E. Scemes, D. C. Spray, and R. Dermietzel. 2000. Evidence for secretory pathway localization of a voltage-dependent anion channel isoform. *Proc. Natl. Acad. Sci. USA.* 97: 3201–3206.

Cantiello, H. F. 2001. Electrodiffusional ATP movement through CFTR and other ABC transporters. *Pflugers Arch.* 443:S22–S27.

Cantiello, H. F., G. R. Jackson, Jr., C. F. Grosman, A. G. Prat, S. C. Borkan, Y. Wang, I. L. Reisin, C. R. O'Riordan, and D. A. Ausiello. 1998. Electrodiffusional ATP movement through the cystic fibrosis transmembrane conductance regulator. *Am. J. Physiol.* 274:C799–C809.

Cantiello, H. F., G. R. Jackson, Jr., A. G. Prat, J. L. Gazley, J. N. Forrest, Jr., and D. A. Ausiello. 1997. cAMP activates an ATP-conductive pathway in cultured shark rectal gland cells. *Am. J. Physiol.* 272:C466–C475.

Carneiro, C. M., O. V. Krasilnikov, L. N. Yuldasheva, A. C. Campos de Carvalho, and R. A. Nogueira. 1997. Is the mammalian porin channel, VDAC, a perfect cylinder in the high conductance state? *FEBS Lett.* 416:187–189.

Carneiro, C. M., P. G. Merzlyak, L. N. Yuldasheva, L. G. Silva, F. P. Thinnes, and O. V. Krasilnikov. 2003. Probing the volume changes

during voltage gating of porin 31BM channel with nonelectrolyte polymers. *Biochim. Biophys. Acta.* 1612:144–153.

Cini, R., M. C. Burla, A. Nunzi, G. P. Polidori, and P. F. Zanazzi. 1984. Preparation and physicochemical properties of the ternary complexes formed between adenosine 5′-triphosphoric acid, bis(2-pyridyl)amine, and divalent metal ions. Crystal and molecular structure of the compounds containing Mg^{++} and Ca^{++}. *J. Chem. Soc. Dalton Trans.* 11:2467–2476.

Colombini, M. 1979. A candidate for the permeability pathway of the outer mitochondrial membrane. *Nature.* 279:643–645.

Dermietzel, R., T. K. Hwang, R. Buettner, A. Hofer, E. Dotzler, M. Kremer, R. Deutzmann, F. P. Thinnes, G. I. Fishman, and D. C. Spray. 1994. Cloning and in situ localization of a brain-derived porin that constitutes a large-conductance anion channel in astrocytic plasma membranes. *Proc. Natl. Acad. Sci. USA.* 91:499–503.

Droogmans, G., C. Maertens, J. Prenen, and B. Nilius. 1999. Sulphonic acid derivatives as probes of pore properties of volume-regulated anion channels in endothelial cells. *Br. J. Pharmacol.* 128:35–40.

Droogmans, G., J. Prenen, J. Eggermont, T. Voets, and B. Nilius. 1998. Voltage-dependent block of endothelial volume-regulated anion channels by calix[4]arenes. *Am. J. Physiol.* 275:C646–C652.

Dubyak, G. R., and C. El-Moatassim. 1993. Signal transduction via P2-purinergic receptors for extracellular ATP and other nucleotides. *Am. J. Physiol.* 265:C577–C606.

Dutta, A. K., Y. Okada, and R. Z. Sabirov. 2002. Regulation of an ATP-conductive large-conductance anion channel and swelling-induced ATP release by arachidonic acid. *J. Physiol. (Lond.).* 542:803–816.

Dwyer, T. M., D. J. Adams, and B. Hille. 1980. The permeability of the endplate channel to organic cations in frog muscle. *J. Gen. Physiol.* 75:469–492.

Eben-Brunnen, J., S. Reymann, L. A. Awni, T. Cole, T. Hellmann, K. P. Hellmann, G. Paetzold, J. Kleineke, F. P. Thinnes, H. Gotz, and N. Hilschmann. 1998. Lentil lectin-enriched microsomes from the plasma membrane of the human B-lymphocyte cell line H2LCL carry a heavy load of type-1 porin. *Biol. Chem.* 379:1419–1426.

Fields, R. D., and B. Stevens. 2000. ATP: an extracellular signaling molecule between neurons and glia. *Trends Neurosci.* 23:625–633.

Finkelstein, A. 1987. Water Movement through Lipid Bilayers, Pores, and Plasma Membranes. Theory and Reality. John Wiley & Sons, New York.

Hazama, A., H. T. Fan, I. Abdullaev, E. Maeno, S. Tanaka, Y. Ando-Akatsuka, and Y. Okada. 2000. Swelling-activated, cystic fibrosis transmembrane conductance regulator-augmented ATP release and Cl^- conductances in murine C127 cells. *J. Physiol. (Lond.).* 523:1–11.

Hazama, A., A. Miwa, T. Miyoshi, T. Shimizu, and Y. Okada. 1998. ATP release from swollen or CFTR expressing epithelial cells. *In* Cell Volume Regulation: The Molecular Mechanism and Volume Sensing Machinery. Y. Okada, editor. Elsevier, Amsterdam, The Netherlands. 93–98.

Hazama, A., T. Shimizu, Y. Ando-Akatsuka, S. Hayashi, S. Tanaka, E. Maeno, and Y. Okada. 1999. Swelling-induced, CFTR-independent ATP release from a human epithelial cell line: lack of correlation with volume-sensitive Cl^- channels. *J. Gen. Physiol.* 114:525–533.

Hille, B. 2001. Ion Channels of Excitable Membranes. 3rd Ed. Sinauer Associates, Sunderland, MA.

Hisadome, K., T. Koyama, C. Kimura, G. Droogmans, Y. Ito, and M. Oike. 2002. Volume-regulated anion channels serve as an auto/paracrine nucleotide release pathway in aortic endothelial cells. *J. Gen. Physiol.* 119:511–520.

Hoebertz, A., T. R. Arnett, and G. Burnstock. 2003. Regulation of bone resorption and formation by purines and pyrimidines. *Trends Pharmacol. Sci.* 24:290–297.

Illek, B., A. W. Tam, H. Fischer, and T. E. Machen. 1999. Anion selectivity of apical membrane conductance of Calu 3 human airway epithelium. *Pflugers Arch.* 437:812–822.

Jakob, C., H. Gotz, T. Hellmann, K. P. Hellmann, S. Reymann, H. Florke, F. P. Thinnes, and N. Hilschmann. 1995. Studies on human porin: XIII. The type-1 VDAC ''porin 31HL'' biotinylated at the plasmalemma of trypan blue excluding human B lymphocytes. *FEBS Lett.* 368:5–9.

Kennard, O., N. W. Isaacs, W. D. S. Motherwell, J. C. Coppola, D. L. Wampler, A. C. Larson, and D. G. Watson. 1971. The crystal and molecular structure of adenosine triphosphate. *Proc. R. Soc. Lond. A.* 325:401–436.

Krasilnikov, O. V. 2002. Sizing channel with polymers. *In* Structure and Dynamics of Confined Polymers. J. J. Kasianowicz, M. S. Z. Kellernayer, and D. W. Deamer, editors. Kluwer, Dordrecht, The Netherlands. 73–91.

Krasilnikov, O. V., C. M. Carneiro, L. N. Yuldasheva, A. C. Campos-de-Carvalho, and R. A. Nogueira. 1996. Diameter of the mammalian porin channel in open and ''closed'' states: direct measurement at the single channel level in planar lipid bilayer. *Braz. J. Med. Biol. Res.* 29:1691–1697.

Krasilnikov, O. V., R. Z. Sabirov, V. I. Ternovsky, P. G. Merzliak, and B. A. Tashmukhamedov. 1988. The structure of *Staphylococcus aureus* α-toxin-induced ionic channel. *Gen. Physiol. Biophys.* 7:467–473.

Krasilnikov, O. V., R. Z. Sabirov, V. I. Ternovsky, P. G. Merzliak, and J. N. Muratkhodjaev. 1992. A simple method for the determination of the pore radius of ion channels in planar lipid bilayer membranes. *FEMS Microbiol. Immunol.* 5:93–100.

Kuga, S. 1981. Pore size distribution analysis of gel substances by size exclusion chromatography. *J. Chromatogr.* 206:449–461.

Lader, A. S., Y. Wang, G. R. Jackson, Jr., S. C. Borkan, and H. F. Cantiello. 2000. cAMP-activated anion conductance is associated with expression of CFTR in neonatal mouse cardiac myocytes. *Am. J. Physiol.* 278:C436–C450.

Linsdell, P., and J. W. Hanrahan. 1998. Adenosine triphosphate-dependent asymmetry of anion permeation in the cystic fibrosis transmembrane conductance regulator chloride channel. *J. Gen. Physiol.* 111:601–614.

Linsdell, P., J. A. Tabcharani, J. M. Rommens, Y. X. Hou, X. B. Chang, L. C. Tsui, J. R. Riordan, and J. W. Hanrahan. 1997. Permeability of wild-type and mutant cystic fibrosis transmembrane conductance regulator chloride channels to polyatomic anions. *J. Gen. Physiol.* 110:355–364.

Mannella, C. A. 1998. Conformational changes in the mitochondrial channel protein, VDAC, and their functional implications. *J. Struct. Biol.* 121:207–218.

Merzlyak, P. G., L. N. Yuldasheva, C. G. Rodrigues, C. M. Carneiro, O. V. Krasilnikov, and S. M. Bezrukov. 1999. Polymeric nonelectrolytes to probe pore geometry: application to the α-toxin transmembrane channel. *Biophys. J.* 77:3023–3033.

Movileanu, L., and H. Bayley. 2001. Partitioning of a polymer into a nanoscopic protein pore obeys a simple scaling law. *Proc. Natl. Acad. Sci. USA.* 98:10137–10141.

Movileanu, L., S. Cheley, and H. Bayley. 2003. Partitioning of individual flexible polymers into a nanoscopic protein pore. *Biophys. J.* 85: 897–910.

Nilius, B., T. Voets, J. Eggermont, and G. Droogmans. 1999. VRAC: a multifunctional volume-regulated anion channel in vascular endothelium. *In* Chloride Channels. R. Kozlowski, editor. Isis Medical Media, Oxford, UK. 47–63.

Novak, I. 2003. ATP as a signaling molecule: the exocrine focus. *News Physiol. Sci.* 18:12–17.

Okada, Y. 1997. Volume expansion-sensing outward-rectifier Cl^- channel: fresh start to the molecular identity and volume sensor. *Am. J. Physiol.* 273:C755–C789.

Pasyk, E. A., and J. K. Foskett. 1997. Cystic fibrosis transmembrane conductance regulator-associated ATP and adenosine 3′-phosphate 5′-phosphosulfate channels in endoplasmic reticulum and plasma membranes. *J. Biol. Chem.* 272:7746–7751.

Ralevic, V., and G. Burnstock. 1998. Receptors for purines and pyrimidines. *Pharmacol. Rev.* 50:413–492.

Ralevic, V., and G. Burnstock. 2003. Involvement of purinergic signaling in cardiovascular diseases. *Drug News Perspect.* 16:133–140.

Reisin, I. L., A. G. Prat, E. H. Abraham, J. F. Amara, R. J. Gregory, D. A. Ausiello, and H. F. Cantiello. 1994. The cystic fibrosis transmembrane conductance regulator is a dual ATP and chloride channel. *J. Biol. Chem.* 269:20584–20591.

Robinson, R. A., and R. H. Stokes. 1959. Electrolyte Solutions, 2nd Ed. Butterworths, London, UK.

Roman, R. M., Y. Wang, S. D. Lidofsky, A. P. Feranchak, N. Lomri, B. F. Scharschmidt, and J. G. Fitz. 1997. Hepatocellular ATP-binding cassette protein expression enhances ATP release and autocrine regulation of cell volume. *J. Biol. Chem.* 272:21970–21976.

Rostovtseva, T. K., and S. M. Bezrukov. 1998. ATP transport through a single mitochondrial channel, VDAC, studied by current fluctuation analysis. *Biophys. J.* 74:2365–2373.

Rostovtseva, T., and M. Colombini. 1997. VDAC channels mediate and gate the flow of ATP: implications for the regulation of mitochondrial function. *Biophys. J.* 72:1954–1962.

Rostovtseva, T. K., A. Komarov, S. M. Bezrukov, and M. Colombini. 2002a. VDAC channels differentiate between natural metabolites and synthetic molecules. *J. Membr. Biol.* 187:147–156.

Rostovtseva, T. K., E. M. Nestorovich, and S. M. Bezrukov. 2002b. Partitioning of differently sized poly(ethylene glycol)s into OmpF porin. *Biophys. J.* 82:160–169.

Sabirov, R. Z., and Y. Okada. 2004. ATP-conducting maxi-anion channel: a new player in stress-sensory transduction. *Jpn. J. Physiol.* 54:7–14.

Sabirov, R. Z., A. K. Dutta, and Y. Okada. 2001. Volume-dependent ATP-conductive large-conductance anion channel as a pathway for swelling-induced ATP release. *J. Gen. Physiol.* 118:251–266.

Sabirov, R. Z., O. V. Krasilnikov, V. I. Ternovsky, and P. G. Merzliak. 1993. Relation between ionic channel conductance and conductivity of media containing different nonelectrolytes. A novel method of pore size determination. *Gen. Physiol. Biophys.* 12:95–111.

Sabirov, R., O. V. Krasilnikov, V. I. Ternovsky, P. G. Merzliak, and J. N. Muratkhodjaev. 1991. Influence of some nonelectrolytes on conductivity of bulk solution and conductance of ion channels. Determination of pore radius from electric measurements. *Biologicheskie Membr.* 8:280–291.

Schein, S. J., M. Colombini, and A. Finkelstein. 1976. Reconstitution in planar lipid bilayers of a voltage-dependent anion-selective channel obtained from *paramecium* mitochondria. *J. Membr. Biol.* 30:99–120.

Schwiebert, E. M., and A. Zsembery. 2003. Extracellular ATP as a signaling molecule for epithelial cells. *Biochim. Biophys. Acta.* 1615:7–32.

Schwiebert, E. M., M. E. Egan, T. H. Hwang, S. B. Fulmer, S. S. Allen, G. R. Cutting, and W. B. Guggino. 1995. CFTR regulates outwardly rectifying chloride channels through an autocrine mechanism involving ATP. *Cell.* 81:1063–1073.

Sigel, H. 1987. Isomeric equilibria in complexes of adenosine 5-triphosphate with divalent metal ions. *Eur. J. Biochem.* 165:65–72.

Soejima, M., and S. Kokubun. 1988. Single anion-selective channel and its ion selectivity in the vascular smooth muscle cell. *Pflugers Arch.* 411:304–311.

Steinacker, P., L. A. Awni, S. Becker, T. Cole, S. Reymann, D. Hesse, H. D. Kratzin, C. Morris-Wortmann, C. Schwarzer, F. P. Thinnes, and N. Hilschmann. 2000. The plasma membrane of *Xenopus laevis* oocytes contains voltage-dependent anion-selective porin channels. *Int. J. Biochem. Cell Biol.* 32:225–234.

Strange, K., F. Emma, and P. S. Jackson. 1996. Cellular and molecular physiology of volume-sensitive anion channels. *Am. J. Physiol.* 270: C711–C730.

Sugita, M., Y. Yue, and J. K. Foskett. 1998. CFTR Cl^- channel and CFTR-associated ATP channel: distinct pores regulated by common gates. *EMBO J.* 17:898–908.

Thinnes, F. P., H. Gotz, H. Kayser, R. Benz, W. E. Schmidt, H. D. Kratzin, and N. Hilschmann. 1989. Identification of human porins. I. Purification of a porin from human B-lymphocytes (Porin 31HL) and the topochemical proof of its expression on the plasmalemma of the progenitor cell. *Biol. Chem. Hoppe Seyler.* 370:1253–1264.

Wunder, U. R., and M. Colombini. 1991. Patch clamping VDAC in liposomes containing whole mitochondrial membranes. *J. Membr. Biol.* 123:83–91.